

Continual Learning in the Presence of Spurious Correlation

Donggyu Lee^{1*}, Sangwon Jung^{2*}, Taesup Moon^{2,3,4†}

¹ Department of Electrical and Computer Engineering, Sungkyunkwan University

² Department of Electrical and Computer Engineering, Seoul National University

³ SNU-LG AI Research Center ⁴ ASRI/INMC/IPAI/AIIS, Seoul National University

ldk3088@skku.edu, {s.jung, tsmoon}@snu.ac.kr

Abstract

Most continual learning (CL) algorithms have focused on tackling the stability-plasticity dilemma, that is, the challenge of preventing the forgetting of previous tasks while learning new ones. However, they have overlooked the impact of the knowledge transfer when the dataset in a certain task is biased — namely, when some unintended spurious correlations of the tasks are learned from the biased dataset. In that case, how would they affect learning future tasks or the knowledge already learned from the past tasks? In this work, we carefully design systematic experiments using one synthetic and two real-world datasets to answer the question from our empirical findings. Specifically, we first show through two-task CL experiments that standard CL methods, which are unaware of dataset bias, can transfer biases from one task to another, both forward and backward, and this transfer is exacerbated depending on whether the CL methods focus on the stability or the plasticity. We then present that the bias transfer also exists and even accumulate in longer sequences of tasks. Finally, we propose a simple, yet strong plug-in method for debiasing-aware continual learning, dubbed as Group-class **B**alanced **G**reedy **S**ampling (BGS). As a result, we show that our BGS can always reduce the bias of a CL model, with a slight loss of CL performance at most.

1. Introduction

Continual learning (CL) is essential for a system that needs to learn (potentially increasing number of) tasks from sequentially arriving data. The main challenge of CL is to overcome the *stability-plasticity* dilemma [36]; when a CL model focuses too much on the stability, it would suffer from low plasticity for learning a new task (and vice versa). Recent deep neural networks (DNNs) based CL methods [22, 16, 27] attempted to address the dilemma by devising

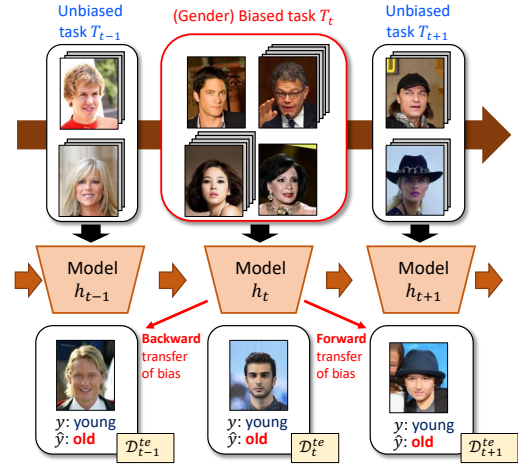


Figure 1: **An illustration for bias transfer in continual learning.** The three tasks sequentially arrive, where each sample contains blond hair, black hair and hat. When a naive CL model is used to update the model h_t from T_t , the gender bias is obtained by the model, and the bias is transferred forward and backward, e.g., the model falsely predicts young man images to “old” class in T_{t-1} and T_{t+1} .

mechanisms to attain stability while improving plasticity thanks to the *knowledge transferability* [45], which is one of the standout properties of DNNs. Namely, while maintaining the learned knowledge, the performance on a new task (resp. past tasks) is improved by transferring knowledge of past tasks (resp. a new task). Such phenomena are called the forward and backward transfer, respectively.

While such DNN-based approaches for CL have been successful to some extent, they have not explicitly considered a more realistic and challenging setting in which the *dataset bias* [49] exists; *i.e.*, a training dataset may contain unintended correlations between some spurious features and class labels. In such a case, it is widely known that DNNs often dramatically fail to generalize to the test data without the correlation due to learning the spurious features [41, 1]. For instance, consider a DNN that can accurately

*Equal contribution.

classify birds in the sky. However, when presented with images of birds outside of their typical sky background, the model may fail due to relying on shortcut strategies that exploit the background [12]. This issue has been the subject of various attempts to resolve it, with earlier approaches [37, 28] often being based on empirical observations of DNN behavior, which yielded suboptimal results.

Now, we claim that the issue of learning spurious correlations in the context of CL can be a significant problem because it can lead to the issue of *bias transfer*. In a recent study [42], it is shown that the bias learned by a model can be (forward) transferred to the downstream model even when it is fine-tuned with unbiased downstream task data. In CL, this issue can be potentially exacerbated since CL involves learning a sequence of tasks, and the bias transfer can occur in both forward and backward directions. For instance, consider an example of domain-incremental learning (Domain-IL) setting shown in Figure 1, in which the goal is to incrementally learn the classifier that predicts whether the face in the image is *young* or not, as the training data arrives. Now, assume that among three tasks, T_{t-1} , T_t and T_{t+1} , only the dataset for T_t possesses the *gender* bias due to the data imbalance; namely, “male” and “female” face tends to spuriously correlate with “old” and “young” class, respectively. We argue that when a naive CL method, which does not concern about the bias transfer, is used to update the model h_t from T_t , the *gender* bias picked up by the model can adversely affect the prediction for the test images in previous or future task, *i.e.*, T_{t-1} or T_{t+1} . In other words, while the models independently trained with T_{t-1} or T_{t+1} would not contain any bias, the naive CL-updated h_t and h_{t+1} can falsely predict the test “male” images for T_{t-1} or T_{t+1} to be “old”, respectively, due to the “gender” bias in h_t transferring to the predictions for past and future tasks. To the best of our knowledge, this issue has not been carefully investigated in the CL research community.

To that end, through systematic and carefully designed experiments, we quantitatively show that the above issue of bias transfer in CL, both forward and backward, indeed exists and significantly affects the model performance. More specifically, using one synthetic and two real-world datasets, we first carry out extensive two-task CL experiments and identify that when a typical CL method focuses on the stability (resp. plasticity), the bias learned from the past task (resp. current task) gets transferred and affects the model learned for the current task (resp. past task). Furthermore, we show such forward and backward bias transfer also exists and even *accumulates* when naively applying CL methods for a longer sequence of tasks with dataset bias. Finally, we present a simple yet strong plug-in method, dubbed as Group-class **B**alanced **G**reedy Sampling (BGS), which can be easily combined with any existing CL methods. Using an class-group balanced exemplar memory,

BGS retrains the last layer of a DNN-based CL model after learning the last task. As a result, we show that our method can always reduce the bias of a CL model with a slight loss of accuracy at most. Despite of our improvements, our results clearly call for a fundamental and novel approach for continually learning each task with potential bias while debiasing the task.

The remainder of this paper is organized as follows. Section 2 discusses some related works for continual and debiasing learning, and 3 introduces the experimental setup. In Section 4, we first investigate the forward and backward transfers of bias in two-task CL scenarios, and in Section 5, further study them in longer sequences of tasks. Then, Section 6 gives a detailed description of BGS and comparison results with other baseline methods.

2. Related works

Continual learning (CL). Assuming that tasks are clearly separated, CL scenarios are typically categorized into three categories: task-incremental learning (Task-IL), domain-incremental learning (Domain-IL), and class-incremental learning (Class-IL) [51]. The Task-IL and Class-IL assume each task has a disjoint set of labels and the task identity is provided during training. The main difference between the two is whether the task identity is used (Task-IL) at test time or not (Class-IL). Task-IL adopts the structure of a multi-headed network with a classification head for each task since it uses the task identity at the test time. In contrast, Class-IL uses a single-headed network due to the lack of task identity at the test time. In Domain-IL, the class set of the tasks always remains the same, but only the input distributions vary as the number of tasks increases.

Recent CL methods can also be classified into three categories based on how they prevent forgetting of the previously learned tasks [8]: rehearsal based, regularization based, and parameter isolation based methods. Regularization based methods add regularization terms for penalizing deviation from past models and balance the stability-plasticity trade-off by controlling the regularization hyperparameter [22, 27, 16, 46]. Rehearsal based methods store some data points from past tasks in a small exemplar memory and replay them while learning the current task [7, 31, 6, 47]. Parameter isolation based methods [40, 35, 34, 15, 54] allocate model parameters separately for each task by masking out previous task parameters and updating only remained parameters for learning a new task. Note that parameter isolation based methods can be applied to only Task-IL settings since they require task identity during inference to separate parameters for each task.

While many state-of-the-art CL methods in each category have been actively developed, many of them were limited for direct application to real-world deployment scenarios. For instance, most existing CL methods focus on learn-

ing well-balanced tasks with reliable labels. To that end, some considered more practical settings; *e.g.*, CL scenarios with imbalanced data [19], noisy labels [20, 2], and dataset bias [25]. While [25] shares a somewhat similar motivation as ours, their overall experimental setup was not sufficiently fine-grained to fully support their own findings.

Spurious correlations and debiased learning. Machine learning community has attempted to comprehend issues of spurious correlations, and as a result, there have been a variety of studies that aim to identify and mitigate various forms of real-world spurious correlations. For instance, in vision tasks, neural networks may rely on background [41, 12], texture [13], or semantically irrelevant features of objects [29] in the image. In addition, numerous approaches to address these issues have been proposed. Early approaches utilize known group labels that indicate the misleadingly correlated attributes, such as background or gender [41, 18]. As an example, Sagawa et al. [41] developed Group DRO which minimizes the worst-case group loss in the training data by using some prior knowledge of spurious correlations. Since annotating group labels is costly, more recent works have developed more practical methods that need only bias type [1], partially annotated group labels [28, 17], or no group labels [37]. Nonetheless, they have not been considered spurious correlations in continual learning.

3. Experimental setup

3.1. Notations and problem setting

We consider the *bias-aware continual learning* which is composed of a sequence of classification tasks which may contain a dataset bias. Each data sample in the t -th task T_t consists of the tuple (x_i, a_i, y_i) where $a_i \in \mathcal{A}$ and $y_i \in \mathcal{Y}_t$ are group and class labels of an input x_i , respectively. Unless otherwise noted, we consider the single type of bias in a CL scenario for simplicity of analysis. In addition, the sets of class label, $\{\mathcal{Y}_i\}_{i \in \{1, 2, \dots\}}$, can be identical or not, depending on the type of CL scenarios.

3.2. Benchmark datasets

We use one synthetic dataset, Split CIFAR-100S, and two real-world datasets, CelebA² (or CelebA⁸) and Split ImageNet-100, which are applied for Task-IL, Domain-IL, and Class-IL settings, respectively. Followings are descriptions for our datasets (more details are in Appendix).

Split CIFAR-100S is a modified dataset from Split CIFAR-100 [55, 7, 50], which randomly divides CIFAR-100 [24] into 10 tasks with 10 distinct classes. Similarly as in [53], we modify split CIFAR-100 such that, given a skew-ratio $\alpha \geq 0.5$, half of the classes in each task are skewed toward the grayscale group and the other half toward the color group; namely, the training images of each class are split into α and $1 - \alpha$ ratios for each group. Thus, the “color”

becomes the bias of the dataset. We set 7 bias levels (0-6) by dividing the range of skew-ratio from 0.5 to 0.99 evenly on a log scale for systematic control of the degree of bias.

CelebA [30] contains more than 200K face images, each annotated with 40 binary attributes. It is notorious for containing representation biases towards specific attributes such as race, age, or gender [48, 10]; for instance, the sub-populations of young women and old men are over-represented in the CelebA dataset. Unless otherwise specified, we use “gender” and “young” attributes as a group and a class label, respectively. We additionally select one or three other attributes and based on them, divide CelebA into two tasks (used in section 4) or eight tasks (used in section 5 and 6), which are denoted as CelebA² or CelebA⁸, respectively. Since the representation bias in CelebA can be controlled by adjusting imbalances between the class and group labels, we set 7 bias levels varying on the degree of imbalance from 0.5 to 0.99, as the same procedure in Split CIFAR-100S.

Split ImageNet-100 divides ImageNet-100 [9] into 10 tasks with disjoint 10 classes which are randomly sampled from original 1000 classes in ImageNet-1000. It is known that DNN models trained from ImageNet are biased towards watermark [44]; namely, the ImageNet-pretrained models predict an image as the carton class when injecting a watermark to it, since most of carton images in the ImageNet training dataset include the watermark. Following the recent study, we also consider the watermark bias in Split ImageNet-100. We utilize two types of test datasets, the original ImageNet validation dataset, and ImageNet-W with watermarks injected by style transfer [26, 11], in order to measure the degree of bias. We set a bias level of a task as 0 or 6, depending on the presence of a carton class in the task.

3.3. Continual learning and debiasing baselines

We compare two naive methods and six representative CL methods: *fine-tuning* without any consideration of CL, *model-freezing* with freezing model parameters updated from previous tasks, LWF [27] and EWC [22] for regularization based methods, ER [7] and iCaRL [39] for rehearsal based methods and PackNet [35] for parameter isolation based methods. We note that each CL method can control the stability-plasticity trade-off by adjusting their own hyperparameters such as the regularization strength, the size of the exemplar memory or the pruning ratio. We further note that PackNet is designed only for task-IL settings, LWF for task-IL and class-IL, and iCaRL for class-IL settings. Additionally, we employ a widely used debiasing technique, Group DRO [41]. For implementation details, please refer to the Appendix.

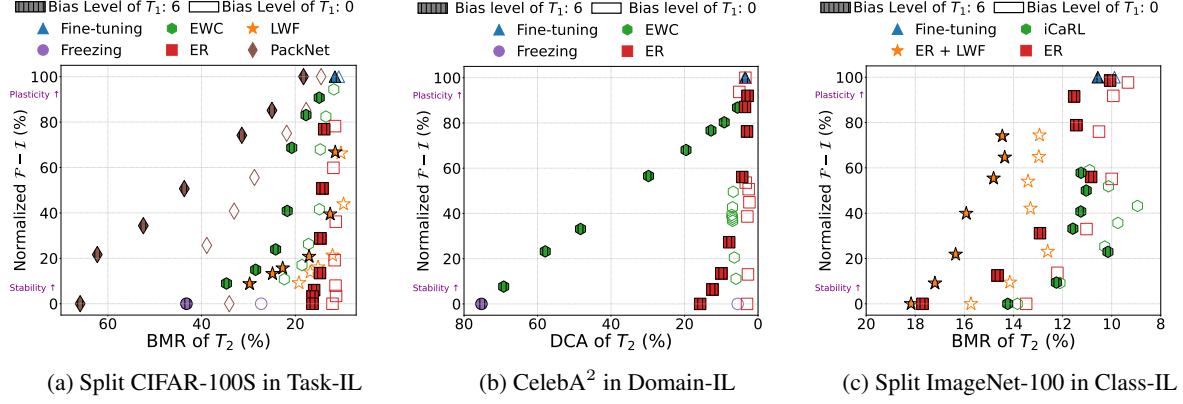


Figure 2: Forward transfer of bias in two tasks-continual learning.

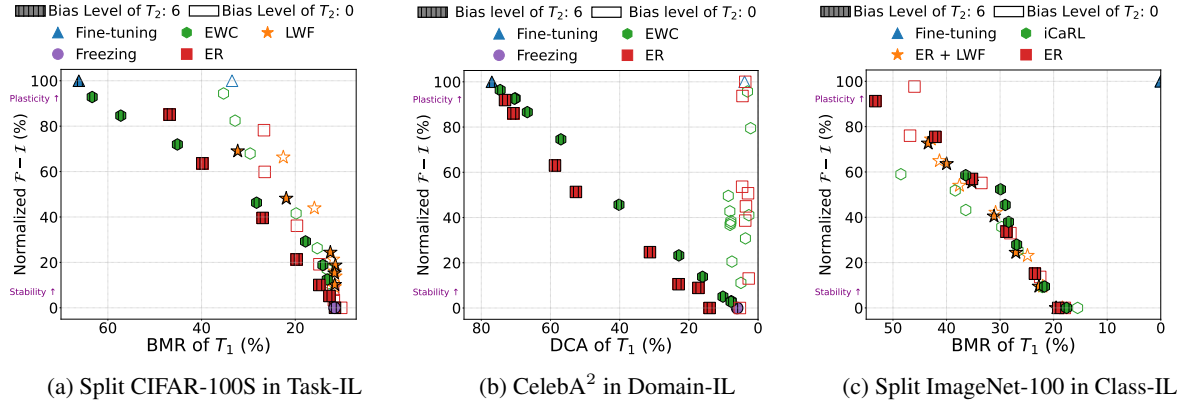


Figure 3: Backward transfer of bias in two tasks-continual learning.

3.4. Metrics

We utilize *average accuracy* over learned tasks as a metric for CL performance and *Normalized $\mathcal{F} - \mathcal{I}$* as a metric for the relative weight on plasticity and stability. The concrete definition of Normalized $\mathcal{F} - \mathcal{I}$ is given below. Let h_t and h_t^* be the classifiers learned up to T_t tasks which are trained by a CL method and the fine-tuning, respectively. The forgetting and intransigence measures [5, 4], \mathcal{F}_t and \mathcal{I}_t , after learning up to task T_t are then defined as follows:

$$\mathcal{F}_t : \frac{1}{t-1} \sum_{j=1}^{t-1} \max_{l \in [t-1]} A(h_l, \mathcal{D}_j) - A(h_t, \mathcal{D}_j) \quad (1)$$

$$\mathcal{I}_t : \frac{1}{t} \sum_{j=1}^t A(h_j^*, \mathcal{D}_j) - A(h_j, \mathcal{D}_j), \quad (2)$$

in which $A(h, \mathcal{D}_t)$ is the test accuracy of a model for a test dataset of T_t , \mathcal{D}_t . Note that the two measures evaluate the stability and plasticity of a CL method, respectively. Then, for each CL scenario and method, the differences between the two measures are normalized by the maximum and minimum values of $\mathcal{F} - \mathcal{I}$, which are obtained by varying the

hyperparameter of each CL method. Especially, in the case of regularization based methods, the maximum and minimum values of $\mathcal{F} - \mathcal{I}$ mostly correspond to $\mathcal{F} - \mathcal{I}$ of the fixed model and the fine-tuning. Notably, the Normalized $\mathcal{F} - \mathcal{I}$ indicates the model focuses more on stability as the value becomes lower and on plasticity as it becomes higher.

The degree of bias of the model can be evaluated by observing its behavior for predicting a sample when a bias feature of the sample is changed. Formally, we measure a model bias using the bias-flipped mis-classification rate (BMR):

$$\text{BMR} = \frac{\sum_{\{x_i \in \mathcal{D} | h(x_i) = y_i\}} \mathbb{I}(h(x_i^*) \neq y_i)}{|\{x_i \in \mathcal{D} | h(x_i) = y_i\}|}, \quad (3)$$

in which x_i^* is a bias-flipped sample with other features fixed, e.g., changes of presence only for color (for Split CIFAR-100S) or watermark (for Split-ImageNet). Namely, BMR considers the number of falsely predicted samples after only flipping bias features for all correctly predicted samples.

In most real-world datasets such as CelebA, it might be challenging to generate bias-flipped samples such as transforming a woman image to look like a man. Thus, for

CelebA, we use the difference of classwise accuracy (DCA) [3] as a surrogate metric:

$$\text{DCA}(h, \mathcal{D}_t) = \frac{1}{|\mathcal{Y}_t|} \sum_{y \in \mathcal{Y}_t} \max_{a, a' \in \mathcal{A}} |A(h, \mathcal{D}_t^{y,a}) - A(h, \mathcal{D}_t^{y,a'})|,$$

in which $\mathcal{D}_t^{y,a}$ is the subset of \mathcal{D}_t that is confined to the samples with class-group label pair (y, a) . DCA means the average (over class) of per-class maximum accuracy difference between domains. Informally, DCA is regarded as an approximation of BMR by calculating the difference of predictions in group levels, not in sample levels.

We note that we use BMR for Split CIFAR-100S and ImageNet-100 and DCA for CelebA. Further note that high BMR and DCA correspond to h possessing large bias.

4. Case for CL with two tasks

We begin our analysis by examining CL scenarios consisting of two tasks in sequence. Our goal is to identify *forward* and *backward* transfers of the bias of a CL model through both quantitative analyses and figure out how the CL methods promote each of these transfers.

4.1. Forward transfer of bias

To investigate the forward transfer of the bias, we evaluated CL methods by varying the degree of bias of T_1 , while that of T_2 is fixed to level 0. Figure 2 reports bias metric values of T_2 along with Normalized $\mathcal{F} - \mathcal{I}$ on three datasets after learning T_2 with two different bias levels of T_1 , *i.e.*, level 0 & 6. In the figure, we plot the results of each CL method by varying their own hyperparameter for controlling the stability-plasticity trade-off. The upper point on each plot represents a lower regularization strength, a smaller memory size, or a lower pruning ratio.

The following are our observations from the figures. First, from the gap of blue triangles in Split CIFAR-100S and Split ImageNet-100 results, we observe that even with simple fine-tuning, the bias of T_1 adversely affects one of T_2 , *i.e.*, forward transfer of bias exists, which is consistent with Salman *et al.* [42]. However, the overlapping blue triangles on CelebA show that the bias of T_1 does not always persist when not considering the stability, implying that the degree of forgetting for the bias of a model acquired from previous tasks can be different depending on the types of bias. Second, we observe that when applying CL methods, the gap between colored and uncolored points for similar Normalized $\mathcal{F} - \mathcal{I}$ is mostly larger than fine-tuning. Moreover, the gap increases as Normalized $\mathcal{F} - \mathcal{I}$ becomes lower. Namely, these results clearly demonstrate that CL methods promote the forward transfer of bias because they tend to remember the knowledge of past tasks even if it contains some bias features. Furthermore, the extent of the transfer is increasing as CL methods focus on stability more. Finally, we

observe that bias of T_2 is mostly better when learned after T_1 with bias level 0 than with bias level 6, under similar Normalized $\mathcal{F} - \mathcal{I}$. Therefore, we argue that before learning a new task, biases of a CL model obtained from previous tasks should be mitigated for learning the new tasks correctly.

We additionally report the results on Split CIFAR-100S when the bias level of T_2 is 2 or 4 in Appendix, and observe similar trends from Figure 2.

4.2. Backward transfer of bias

Now, we investigate the backward transfer of bias. Figure 3 compares the bias of a model at T_1 by varying the bias of T_2 , while the bias level of T_1 is fixed as level 0. We omit the results for PackNet, as it freezes the parameters updated in the previous tasks and thereby the predictions for previous tasks are not changed, *i.e.*, any backward transfer does not occur.

Figure 3a and 3b show the opposite trend of our previous results. Firstly, we observe that the bias gap for T_1 under similar Normalized $\mathcal{F} - \mathcal{I}$ is maximized by fine-tuning and minimized by model-freezing. Also, for each CL method, the gap becomes severer as the Normalized $\mathcal{F} - \mathcal{I}$ increases. This means that the more CL methods prioritize plasticity over stability, the more bias obtained from T_2 is transferred to T_1 , *i.e.*, the backward transfer of bias occurs more. Additionally, when the bias level of T_2 is 0, T_1 consistently exhibits lower bias, highlighting the need to address the potential bias of new incoming tasks.

We identify that BMRs between colored and uncolored points are nearly identical in Figure 3c. To reason about this phenomenon, we analyzed the predictions from models and found out that it may be due to the old-new bias which is an inherent issue of Class-IL — namely, predictions are biased towards new classes due to the imbalance between old and new task data samples. In other words, although T_2 does not contain the carton class, the converted image containing watermarks can be predicted to one of the new classes, leading to no difference in BMR. Please refer to Appendix for the related experimental results and more discussions.

Remarks on developing a new CL method. From two-task analyses in Figure 2 and 3, we observed that the bias of each task negatively affects the other tasks even if they do not contain the bias. This appeals that whenever we encounter a bias of an incoming task, we should consider learning the task without the bias and preventing forgetting of the previous tasks at the same time. As a straightforward solution, one may naively consider applying an existing debiasing technique (*e.g.*, Group DRO) to the model obtained after learning a current task by a CL method. However, we can easily expect that the accuracy of previous tasks significantly drops whereas the bias of the current task can be successfully reduced (we report the results of this scenario in

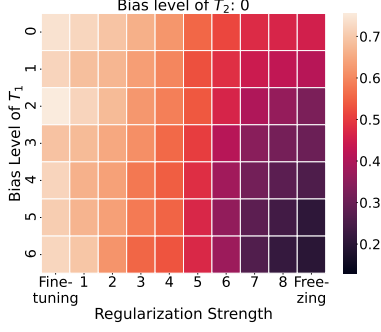


Figure 4: **CKA on Split CIFAR-100S.** To observe the forward transfer of bias, the CKA between color and grayscale images in T_2 is shown according to the bias level of T_1 and the regularization strength, after learning up to T_2 by EWC.

Appendix). Hence, we argue that it is necessary to develop a novel approach for taking debiased learning into account while continual learning.

4.3. Feature representation analysis

To provide more direct evidence of bias transfer, we analyze feature representations extracted from the penultimate layer of a DNN-based model using centered kernel alignment (CKA) with the linear kernel [23]. CKA is an isotropic scaling-invariant metric for measuring the similarity between two representations of a model. The two plots in Figure 4 compare the CKA values on Split CIFAR-100S for EWC under the two-tasks settings similar to Figure 2a. Namely, we evaluate models after learning T_2 by varying the regularization strength and the bias level of T_1 . We then compute the CKA similarity between color and grayscale images in the test dataset of T_2 . That means, a low CKA value indicates that representations for each group are different, *i.e.*, the model possesses the color bias more. Figure 4 clearly shows that as the regularization strength is stronger and the bias of T_1 is more severe, CKA values decrease. Thus, we also observe the forward transfer of the bias through the analysis of feature representations. The CKA result showing the backward transfer is reported in Appendix.

5. Case for CL with a longer sequence of tasks

We confirmed in the previous section that the bias is transferred forward and backward in tow-tasks CL scenarios. In this section, we further investigate the bias transferability in a sequence of multiple tasks.

We note that for all figures in this section, we simplify the visual format for better clarity of the comparison; in detail, we divide a range of the normalized $\mathcal{F} - \mathcal{I}$ into three equal intervals and report a result for each interval. Given a CL scenario, we evaluate CL methods several times for varying their hyperparameters and select one of the results

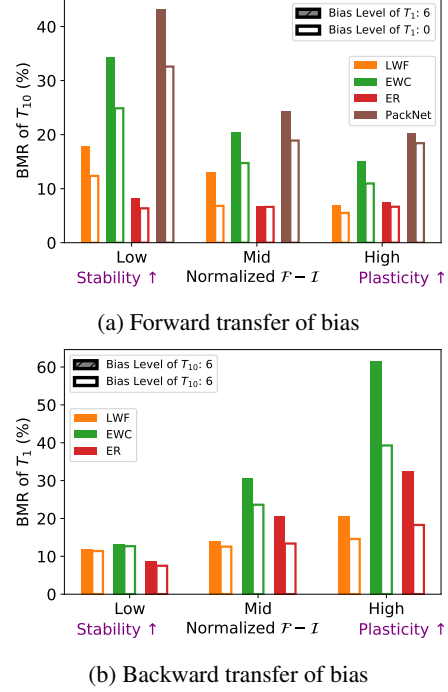


Figure 5: **Bias transfers in a sequence of 10 tasks on Split-CIFAR100S.** The BMRs of T_{10} or T_1 are shown after learning up to T_{10} by CL methods.

with the highest average accuracy for each interval.

5.1. Persistence of bias transfer in longer sequences

Firstly, we consider a sequence of 10 tasks on Split CIFAR-100S to observe that the bias transfer exists in longer CL scenarios. Similar to settings in Figure 2, we vary the bias level of the first or last task with level 0 or 6, while the bias level of all other tasks is fixed as level 0. The two plots in Figure 5 show BMR of T_{10} (resp. T_1) according to the bias of T_1 (resp. T_{10}) for each CL method.

Figure 5 reveals an analogous trend with two-task analyses. Specifically, the two plots exhibit the BMR of T_{10} (resp. T_1) always higher when the bias level of T_1 (resp. T_{10}) is 6. Furthermore, the gap of BMR between them is at its widest when the normalized $\mathcal{F} - \mathcal{I}$ is low (resp. high). Namely, the bias transfers also occur in longer sequences of tasks. We additionally display the accuracy of T_{10} and T_1 for each plot in Appendix and find that the accuracies are roughly the same, meaning that the gap of BMR is due to the bias transfer. Finally, we emphasize that from Figure 5a, the color bias of T_1 can *persist* even if a CL model learns nine additional tasks with the bias level of 0, especially when focusing on the stability.

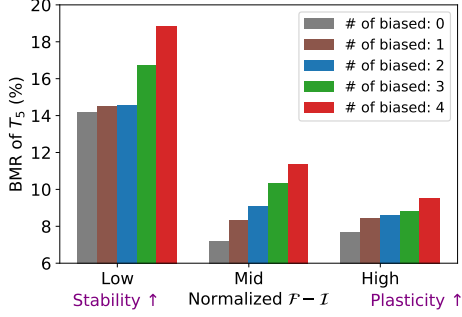


Figure 6: **Accumulation of the same type of bias on Split CIFAR-100S.** BMR of T_5 is shown depending on the number of biased tasks after up to learning T_5 by LWF.

5.2. Accumulation of the same type of bias

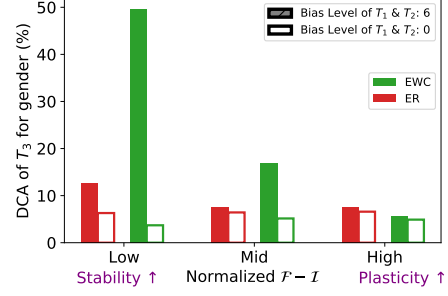
We now verify whether the *same* type of bias of each task would be *accumulated* by CL methods; namely, when the number of previous tasks with the same type of dataset bias is increasing, the CL models make much more biased predictions for the current task. To this end, we take a sequence of 5 tasks with a bias level of 0 in Split CIFAR-100S. We then randomly select some of the four tasks except the last task and change the bias level of them to 4.

Figure 6 reports BMR values for LWF depending on the number of biased tasks. We clearly check that the BMR of T_5 increases as the number of biased tasks increases, and the increase is more significant in the low and middle ranges. Namely, it demonstrates that when tasks with the same type of bias are continuously upcoming, their biases accumulate in the CL model. In addition, we observe that when the number of biased tasks is low in the low range, the gap of BMR is small. It would be because if only the tasks in the middle of sequences have the dataset bias, their dataset bias could not be sufficiently learned under the low plasticity.

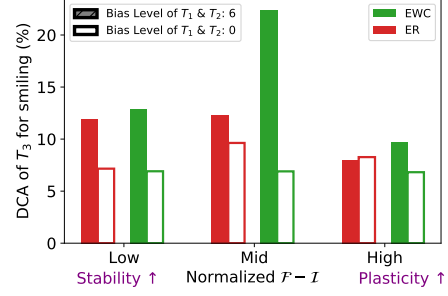
5.3. Accumulation of the different types of bias

In order to investigate that the *different* type of biases can also accumulate, we consider sequences of three tasks, each randomly picked from CelebA⁸. We suppose that each task can include one of two kinds of dataset bias. That is, in the training datasets of each task, the class attribute, “young”, can spuriously correlate with one of two group attributes, “gender” or “smiling”. Then, when bias levels of T_3 for both group attributes are fixed to 0, we compare the BMRs of T_3 depending on whether or not T_1 and T_2 have gender or smiling biases, respectively.

The results are shown in Figure 7, which displays the degree of gender and smiling bias at T_3 for EWC and ER. We find that when T_1 and T_2 are biased towards gender and smiling, respectively, BMR at T_3 are much higher in terms of both group attributes. Moreover, in most cases, we again observe the stronger forward transfer of bias when



(a) DCA of T_3 for the gender bias



(b) DCA of T_3 for the smiling bias

Figure 7: **Accumulation of different types of bias on CelebA⁸.** DCAs of T_3 for “gender” and “smiling” attributes are reported.

CL methods focus on the stability more. In Figure 7b, the gap between colored and uncolored bars for EWC is bigger in the middle range, compared to the low range. We infer that this would be because the dataset bias of T_2 could be learned more under higher plasticity, resulting in the bias being more transferred to T_3 .

6. Bias-aware Continual learning

We demonstrated that the bias of each task can be transferred by naive CL methods in various continual learning situations, highlighting the need for a new approach to continual learning that considers debiasing each task. To address this need, we propose a simple, yet efficient baseline method, dubbed as Group-class **B**alanced **G**reedy Sampling (BGS), that can be easily combined with existing CL methods while preventing forgetting of the learned tasks.

6.1. Group-class Balanced Greedy Sampling (BGS)

Our proposed method is inspired by a recent CL and debiasing method, specifically GDumb (Greedy Sampler and Dumb Learner) [38] and DFR (Deep Feature Re-weighting) [21]. GDumb greedily stores a small number of data into an exemplar memory equally for each class in all tasks and uses them to train a model from scratch during the test time. By learning all tasks at the same time, GDumb can improve the average accuracy over learned tasks. On the other hand, DFR retraining only the classification head us-

Table 1: **The comparison of methods on Split CIFAR-100S.** The average accuracy and BMR over 10 tasks are shown. The k denotes the size of exemplar memory, and the numbers in parentheses stand for the standard deviations of each result obtained with different seeds.

Method	Avg. Acc. (%)	Avg. BMR (%)
Fine-tuning	19.49 (1.46)	51.96 (10.96)
+ BGS (k=1000)	42.75 (2.27)	34.38 (5.70)
+ BGS (k=2000)	47.44 (2.80)	30.42 (5.71)
LWF [27]	59.61 (2.04)	28.00 (2.38)
+ BGS (k=1000)	65.00 (1.20)	18.18 (0.84)
+ BGS (k=2000)	66.88 (1.02)	16.82 (0.90)
EWC [22]	35.57 (1.71)	46.65 (2.31)
+ BGS (k=1000)	46.20 (1.08)	31.65 (2.12)
+ BGS (k=2000)	49.30 (1.37)	28.49 (1.84)
ER (k=1000) [7]	54.77 (1.68)	29.17 (3.81)
+ BGS	59.38 (0.98)	20.89 (2.28)
ER (k=2000)	60.75 (1.12)	25.47 (1.41)
+ BGS	65.00 (0.74)	17.62 (1.46)
PackNet [35]	47.46 (1.52)	33.97 (6.10)
+ BGS (k=1000)	47.69 (2.88)	31.26 (3.93)
+ BGS (k=2000)	49.39 (2.86)	29.15 (4.05)
GDumb (k=1000) [38]	32.33 (1.98)	52.15 (4.95)
GDumb (k=2000)	41.31 (1.99)	45.43 (3.56)
LWF + Group DRO [41]	59.39 (1.41)	23.35 (2.72)

ing a small number of group-balanced data after training a model from scratch using an entire training data that may contain any dataset bias. The authors demonstrate that even if the model learned the biased feature representations, DFR can remove them by only re-training the last layer using a small portion of group-balanced data. We emphasize that both methods are simple to implement and easily applicable to various settings, and can achieve better or comparable performance for CL or debiasing, respectively, compared to more complex and recent methods in its literature.

In a similar spirit, the algorithm of our BGS is two steps: first, during CL using a employed typical CL method, BGS stores group-class balanced data over all seen classes and groups in a greedy manner as the same process as GDumb, which shown is in Appendix. BGS then retrains only the classification heads of a neural network trained by the CL method by using the group-class balanced exemplar memory. By doing this process, we expect that BGS can mitigate the bias of the model like DFR while preventing forgetting of previous tasks. Moreover, we emphasize that BGS can be used in conjunction with any existing CL method without any additional hyperparameters.

6.2. Performance comparison

We evaluate our BGS using 10-task sequences on Split CIFAR-100S and 8-task sequences on CelebA⁸. Each task has a random bias level ranging from 0 to 6 (we did not conduct experiments on Split ImageNet-100 due to the lack of

Table 2: **The comparison of methods on CelebA⁸.** The other settings are identical to Table 1. If there is an improvement by BGS, the result is shown in bold.

Method	Avg. Acc. (%)	Avg. DCA (%)
Fine-tuning	79.77 (1.06)	34.31 (7.53)
+ BGS (k=320)	79.62 (1.24)	31.42 (7.04)
+ BGS (k=640)	79.33 (1.86)	30.30 (6.95)
EWC [22]	80.19 (1.4)	36.30 (9.8)
+ BGS(k=320)	79.15 (2.10)	33.87 (11.74)
+ BGS (k=640)	78.98 (1.72)	32.70 (11.64)
ER (k=320) [7]	80.99 (0.74)	37.68 (6.51)
+ BGS (k=320)	80.19 (1.89)	31.04 (5.11)
ER (k=640)	81.00 (0.80)	37.50 (5.92)
+ BGS (k=640)	79.98 (1.50)	30.49 (2.54)
GDumb (k=320) [38]	69.38 (1.19)	36.45 (5.54)
GDumb (k=640)	72.55 (1.26)	42.25 (1.48)
EWC + Group DRO [41]	75.32 (3.58)	21.79 (3.98)

group labels (*i.e.*, watermark labels) in the training dataset). We compare the standard CL methods including GDumb, and combinations with the CL methods and BGS. Additionally, we evaluate naive combination with the best performing regularization CL method for each dataset and a debiasing technique, Group DRO. We tuned the hyperparameters for each CL method and Group DRO based on the average accuracy and BMR up to T_3 , following the hyperparameter selection protocol used in [33] and used them to learn the rest of the tasks.

Table 1 and 2 present the average accuracy and BMR over all tasks for each method on Split CIFAR-100S and CelebA⁸. We evaluate replay based methods, ER, GDumb, and BGS, with the two kinds of memory size, which correspond to 10 or 20 images per class, respectively. From the tables, we first observe that applying BGS into the standard CL methods leads to improve BMR in all cases and the average accuracy on Split CIFAR-100S, while slightly dropping the average accuracy on CelebA. In addition, we obviously see that the performance gain by BGS in terms of CL and debiasing performances increases when using a large exemplar memory. We emphasize that such improvements from BGS require any additional hyperparameter tuning for debiasing. On the other hand, although applying Group DRO to CL methods shows good performance on CelebA⁸ in terms of BMR, it needs additional hyperparameter tuning for Group DRO, which may be prohibitive for practice. Moreover, we observet that its improvement is marginal on Split CIFAR-100S since LWF + Group DRO may fail to find a good hyperparameter for Group DRO when tuning it with only three tasks, not ten tasks.

Remarks for limitations. Although we demonstrated that BGS can improve average bias metric values in CL scenarios without requiring additional hyperparameter, it is important to note that our method does not fundamentally solve

the bias-aware CL problem. Namely, even with BGS, the feature representation of a CL model could be still biased. Furthermore, BGS does not work in the absence of group labels in the training dataset, such as Split ImageNet-100. Nevertheless, we hope that BGS serves the purpose of a standard baseline for the bias-aware CL problems.

7. Concluding remark

With systematical analyses for two-task and multiple-task CL scenarios, we showed the bias can be transferred both forward and backward by typical CL methods that are oblivious to the dataset bias. Furthermore, we appealed to the CL research community to pay attention to the bias-aware CL problem by exhibiting our in-depth analyses, and proposed a simple baseline method for this problem. For future work, we will develop a more principled approach which can accomplish continual learning and debiasing simultaneously.

References

- [1] Hyojin Bahng, Sanghyuk Chun, Sangdoo Yun, Jaegul Choo, and Seong Joon Oh. Learning de-biased representations with biased representations. In *International Conference on Machine Learning (ICML)*, 2020. 1, 3
- [2] Jihwan Bang, Hyunseo Koh, Seulki Park, Hwanjun Song, Jung-Woo Ha, and Jonghyun Choi. Online continual learning on a contaminated data stream with blurry task boundaries. In *Proceedings of the IEEE/CVF Conference on Computer Vision and Pattern Recognition*, pages 9275–9284, 2022. 3
- [3] Richard Berk, Hoda Heidari, Shahin Jabbari, Michael Kearns, and Aaron Roth. Fairness in criminal justice risk assessments: The state of the art. *Sociological Methods & Research*, 50(1):3–44, 2021. 5
- [4] Sungmin Cha, Hsiang Hsu, Taebaek Hwang, Flavio Calmon, and Taesup Moon. Cpr: Classifier-projection regularization for continual learning. In *International Conference on Learning Representations (ICLR)*, 2021. 4
- [5] Arslan Chaudhry, Puneet K. Dokania, Thalaiyasingam Ajanthan, and Philip H. S. Torr. Riemannian walk for incremental learning: Understanding forgetting and intransigence. In *European Conference on Computer Vision (ECCV)*, September 2018. 4
- [6] Arslan Chaudhry, Marc’Aurelio Ranzato, Marcus Rohrbach, and Mohamed Elhoseiny. Efficient lifelong learning with a gem. In *ICLR*, 2019. 2
- [7] Arslan Chaudhry, Marcus Rohrbach, Mohamed Elhoseiny, Thalaiyasingam Ajanthan, Puneet K Dokania, Philip HS Torr, and Marc’Aurelio Ranzato. Continual learning with tiny episodic memories. *arXiv preprint arXiv:1902.10486*, 2019. 2, 3, 8, 12, 13
- [8] Matthias De Lange, Rahaf Aljundi, Marc Masana, Sarah Parisot, Xu Jia, Aleš Leonardis, Gregory Slabaugh, and Tinne Tuytelaars. A continual learning survey: Defying forgetting in classification tasks. *IEEE transactions on pattern analysis and machine intelligence*, 44(7):3366–3385, 2021. 2
- [9] Jia Deng, Wei Dong, Richard Socher, Li-Jia Li, Kai Li, and Li Fei-Fei. Imagenet: A large-scale hierarchical image database. In *IEEE Conference on Computer Vision and Pattern Recognition*, pages 248–255, 2009. 3
- [10] Simone Fabbrizzi, Symeon Papadopoulos, Eirini Ntoutsi, and Ioannis Kompatsiaris. A survey on bias in visual datasets. *Computer Vision and Image Understanding*, 223:103552, 2022. 3
- [11] Leon A Gatys, Alexander S Ecker, and Matthias Bethge. Image style transfer using convolutional neural networks. In *Proceedings of the IEEE conference on computer vision and pattern recognition*, pages 2414–2423, 2016. 3
- [12] Robert Geirhos, Jörn-Henrik Jacobsen, Claudio Michaelis, Richard Zemel, Wieland Brendel, Matthias Bethge, and Felix A Wichmann. Shortcut learning in deep neural networks. *Nature Machine Intelligence*, 2(11):665–673, 2020. 2, 3
- [13] Robert Geirhos, Patricia Rubisch, Claudio Michaelis, Matthias Bethge, Felix A Wichmann, and Wieland Brendel. Imagenet-trained CNNs are biased towards texture; increasing shape bias improves accuracy and robustness. In *International Conference on Learning Representations*, 2019. 3
- [14] Kaiming He, Xiangyu Zhang, Shaoqing Ren, and Jian Sun. Deep residual learning for image recognition. In *IEEE Conference on Computer Vision and Pattern Recognition (CVPR)*, 2016. 12
- [15] Ching-Yi Hung, Cheng-Hao Tu, Cheng-En Wu, Chien-Hung Chen, Yi-Ming Chan, and Chu-Song Chen. Compacting, picking and growing for unforgetting continual learning. *Advances in Neural Information Processing Systems*, 32, 2019. 2
- [16] Sangwon Jung, Hongjoon Ahn, Sungmin Cha, and Taesup Moon. Continual learning with node-importance based adaptive group sparse regularization. In *Advances in Neural Information Processing Systems (NeurIPS)*, 2020. 1, 2
- [17] Sangwon Jung, Sanghyuk Chun, and Taesup Moon. Learning fair classifiers with partially annotated group labels. In *Proceedings of the IEEE/CVF Conference on Computer Vision and Pattern Recognition*, pages 10348–10357, 2022. 3
- [18] Sangwon Jung, Donggyu Lee, Taeon Park, and Taesup Moon. Fair feature distillation for visual recognition. In *IEEE/CVF Conference on Computer Vision and Pattern Recognition (CVPR)*, 2021. 3
- [19] Chris Dongjoo Kim, Jinseo Jeong, and Gunhee Kim. Imbalanced continual learning with partitioning reservoir sampling. In *Computer Vision–ECCV 2020: 16th European Conference, Glasgow, UK, August 23–28, 2020, Proceedings, Part XIII 16*, pages 411–428. Springer, 2020. 3
- [20] Chris Dongjoo Kim, Jinseo Jeong, Sangwoo Moon, and Gunhee Kim. Continual learning on noisy data streams via self-purified replay. In *Proceedings of the IEEE/CVF international conference on computer vision*, pages 537–547, 2021. 3
- [21] Polina Kirichenko, Pavel Izmailov, and Andrew Gordon Wilson. Last layer re-training is sufficient for robustness to spurious correlations. *arXiv preprint arXiv:2204.02937*, 2022. 7

- [22] J Kirkpatrick, R Pascanu, N Rabinowitz, J Veness, G Desjardins, AA Rusu, K Milan, J Quan, T Ramalho, A Grabska-Barwinska, et al. Overcoming catastrophic forgetting in neural networks. *Proceedings of the National Academy of Sciences of the United States of America*, 114(13):3521–3526, 2017. [1](#), [2](#), [3](#), [8](#), [12](#), [13](#)
- [23] Simon Kornblith, Mohammad Norouzi, Honglak Lee, and Geoffrey Hinton. Similarity of neural network representations revisited. In *International Conference on Machine Learning*, pages 3519–3529. PMLR, 2019. [6](#)
- [24] Alex Krizhevsky. Learning multiple layers of features from tiny images. *Master’s thesis, University of Toronto*, 2009. [3](#)
- [25] Timothée Lesort. Continual feature selection: Spurious features in continual learning. *arXiv preprint arXiv:2203.01012*, 2022. [3](#)
- [26] Zhiheng Li, Ivan Evtimov, Albert Gordo, Caner Hazirbas, Tal Hassner, Cristian Canton Ferrer, Chenliang Xu, and Mark Ibrahim. A whac-a-mole dilemma: Shortcuts come in multiples where mitigating one amplifies others. *arXiv preprint arXiv:2212.04825*, 2022. [3](#), [14](#)
- [27] Zhizhong Li and Derek Hoiem. Learning without forgetting. *IEEE Transactions on Pattern Analysis and Machine Intelligence*, 40(12):2935–2947, 2017. [1](#), [2](#), [3](#), [8](#), [12](#), [13](#)
- [28] Evan Z Liu, Behzad Haghighi, Annie S Chen, Aditi Raghunathan, Pang Wei Koh, Shiori Sagawa, Percy Liang, and Chelsea Finn. Just train twice: Improving group robustness without training group information. In *International Conference on Machine Learning (ICML)*, 2021. [2](#), [3](#)
- [29] Ruyang Liu, Hao Liu, Ge Li, Haodi Hou, Tinghao Yu, and Tao Yang. Contextual debiasing for visual recognition with causal mechanisms. In *IEEE/CVF Conference on Computer Vision and Pattern Recognition (CVPR)*, 2022. [3](#)
- [30] Ziwei Liu, Ping Luo, Xiaogang Wang, and Xiaoou Tang. Deep learning face attributes in the wild. In *Int. Conf. Comput. Vis.*, pages 3730–3738, 2015. [3](#)
- [31] David Lopez-Paz and Marc’Aurelio Ranzato. Gradient episodic memory for continual learning. *Advances in neural information processing systems*, 30, 2017. [2](#)
- [32] Ilya Loshchilov and Frank Hutter. Decoupled weight decay regularization. In *7th International Conference on Learning Representations, ICLR 2019, New Orleans, LA, USA, May 6-9, 2019*. OpenReview.net, 2019. [12](#)
- [33] Zheda Mai, Ruiwen Li, Jihwan Jeong, David Quispe, Hyunwoo Kim, and Scott Sanner. Online continual learning in image classification: An empirical survey. *Neurocomputing*, 469:28–51, 2022. [8](#)
- [34] Arun Mallya, Dillon Davis, and Svetlana Lazebnik. Piggyback: Adapting a single network to multiple tasks by learning to mask weights. In *Proceedings of the European Conference on Computer Vision (ECCV)*, pages 67–82, 2018. [2](#)
- [35] Arun Mallya and Svetlana Lazebnik. Packnet: Adding multiple tasks to a single network by iterative pruning. In *Proceedings of the IEEE conference on Computer Vision and Pattern Recognition*, pages 7765–7773, 2018. [2](#), [3](#), [8](#), [12](#), [13](#)
- [36] Martial Mermillod, Aurélie Bugaiska, and Patrick Bonin. The stability-plasticity dilemma: Investigating the continuum from catastrophic forgetting to age-limited learning effects. *Frontiers in Psychology*, 4:504, 2013. [1](#)
- [37] Junhyun Nam, Hyuntak Cha, Sungsoo Ahn, Jaeho Lee, and Jinwoo Shin. Learning from failure: De-biasing classifier from biased classifier. In *Advances in Neural Information Processing Systems (NeurIPS)*, 2020. [2](#), [3](#)
- [38] Ameya Prabhu, Philip HS Torr, and Puneet K Dokania. Gdumb: A simple approach that questions our progress in continual learning. In *Computer Vision–ECCV 2020: 16th European Conference, Glasgow, UK, August 23–28, 2020, Proceedings, Part II 16*, pages 524–540. Springer, 2020. [7](#), [8](#)
- [39] Sylvestre-Alvise Rebuffi, Alexander Kolesnikov, Georg Sperl, and Christoph H Lampert. icarl: Incremental classifier and representation learning. In *Proceedings of the IEEE conference on Computer Vision and Pattern Recognition*, pages 2001–2010, 2017. [3](#), [12](#), [13](#)
- [40] Andrei A Rusu, Neil C Rabinowitz, Guillaume Desjardins, Hubert Soyer, James Kirkpatrick, Koray Kavukcuoglu, Razvan Pascanu, and Raia Hadsell. Progressive neural networks. *arXiv preprint arXiv:1606.04671*, 2016. [2](#)
- [41] Shiori Sagawa, Pang Wei Koh, Tatsunori B Hashimoto, and Percy Liang. Distributionally robust neural networks. In *International Conference on Learning Representations (ICLR)*, 2020. [1](#), [3](#), [8](#), [13](#), [14](#)
- [42] Hadi Salman, Saachi Jain, Andrew Ilyas, Logan Engstrom, Eric Wong, and Aleksander Madry. When does bias transfer in transfer learning? *arXiv preprint arXiv:2207.02842*, 2022. [2](#), [5](#)
- [43] Jonathan Schwarz, Wojciech Czarnecki, Jelena Luketina, Agnieszka Grabska-Barwinska, Yee Whye Teh, Razvan Pascanu, and Raia Hadsell. Progress & compress: A scalable framework for continual learning. In *International conference on machine learning*, pages 4528–4537. PMLR, 2018. [12](#)
- [44] Sahil Singla and Soheil Feizi. Salient imagenet: How to discover spurious features in deep learning? *arXiv preprint arXiv:2110.04301*, 2021. [3](#)
- [45] Chuanqi Tan, Fuchun Sun, Tao Kong, Wenchang Zhang, Chao Yang, and Chunfang Liu. A survey on deep transfer learning. In *International Conference on Artificial Neural Networks (ICANN)*, 2018. [1](#)
- [46] Michalis K Titsias, Jonathan Schwarz, Alexander G de G Matthews, Razvan Pascanu, and Yee Whye Teh. Functional regularisation for continual learning with gaussian processes. In *International Conference on Learning Representations (ICLR)*, 2020. [2](#)
- [47] Rishabh Tiwari, Krishnateja Killamsetty, Rishabh Iyer, and Pradeep Shenoy. Gcr: Gradient coreset based replay buffer selection for continual learning. In *Proceedings of the IEEE/CVF Conference on Computer Vision and Pattern Recognition*, pages 99–108, 2022. [2](#)
- [48] Robert Torfason, Eirikur Agustsson, Rasmus Rothe, and Radu Timofte. From face images and attributes to attributes. In *Computer Vision–ACCV 2016: 13th Asian Conference on Computer Vision, Taipei, Taiwan, November 20–24, 2016, Revised Selected Papers, Part III 13*, pages 313–329. Springer, 2017. [3](#)

- [49] A Torralba and AA Efros. Unbiased look at dataset bias. In *IEEE/CVF Conference on Computer Vision and Pattern Recognition (CVPR)*, 2011. 1
- [50] Gido M van de Ven, Hava T Siegelmann, and Andreas S Tolias. Brain-inspired replay for continual learning with artificial neural networks. *Nature Communications*, 11:4069, 2020. 3
- [51] Gido M Van de Ven and Andreas S Tolias. Three scenarios for continual learning. *arXiv preprint arXiv:1904.07734*, 2019. 2
- [52] Jeffrey S Vitter. Random sampling with a reservoir. *ACM Transactions on Mathematical Software (TOMS)*, 11(1):37–57, 1985. 12
- [53] Zeyu Wang, Klint Qinami, Ioannis Christos Karakozis, Kyle Genova, Prem Nair, Kenji Hata, and Olga Russakovsky. Towards fairness in visual recognition: Effective strategies for bias mitigation. In *IEEE Conference on Computer Vision and Pattern Recognition (CVPR)*, 2020. 3
- [54] Fei Ye and Adrian G Bors. Lifelong infinite mixture model based on knowledge-driven dirichlet process. In *Proceedings of the IEEE/CVF International Conference on Computer Vision*, pages 10695–10704, 2021. 2
- [55] Friedemann Zenke, Ben Poole, and Surya Ganguli. Continual learning through synaptic intelligence. In *International Conference on Machine Learning (ICML)*, 2017. 3

Appendix

We offer supplementary materials in this document. Specifically, we provide the detailed algorithm of BGS in Section A. In Section B, we present implementation details including model architectures, optimization, implementations of baseline methods, and the range of hyperparameters used. In addition, we report some additional results for a naive debiasing scenario in Section C and other various settings in Section D. Finally, we discuss the results of our study for the backward transfer on Split ImageNet-100 in Section E.

A. BGS sampling algorithm

Algorithm 1: Group-class Balanced Greedy Sampling

Init : Memory $\mathcal{M} = \{\{\}, \dots\}$ with capacity K , Labels $\mathcal{L} = \{\}$, Count $C = \{0, \dots\}$
Input : a data sample (x_i, a_i, y_i) , task id t
Output: \mathcal{M}

```

1  $k \leftarrow \frac{K}{|\mathcal{L}| \times |\mathcal{A}|}$ ;
2 if  $C[(a_i, y_i, t)] < k$  then
3   if  $\sum_{a \in \mathcal{A}, (y, t) \in \mathcal{L}} C[(a, y, t)] < K$  then
4      $\mathcal{M}[(a_i, y_i, t)] = \mathcal{M}[(a_i, y_i, t)] \cup (x_i, a_i, y_i, t)$ ;
5   else
6      $(a_j, y_j, t_j) = \operatorname{argmax}_{(a, y, t)} C[(a, y, t)]$ ;
7      $\mathcal{M}[(a_j, y_j, t_j)] \cdot \text{pop}()$ ;
8      $\mathcal{M}[(a_i, y_i, t)] = \mathcal{M}[(a_i, y_i, t)] \cup (x_i, a_i, y_i, t)$ ;
9      $C[(a_j, y_j, t_j)] = C[(a_j, y_j, t_j)] - 1$ ;
10  end
11  if  $C[(a_i, y_i, t)] == 0$  then
12     $\mathcal{L} = \mathcal{L} \cup (y_i, t)$ ;
13  end
14   $C[(a_i, y_i, t)] = C[(a_i, y_i, t)] + 1$ ;
15 end

```

B. More implementation details

B.1. Model architectures and optimization

For all datasets, we used the AdamW optimizer [32] with the following hyperparameters: learning rate of 0.001, weight decay of 0.01, β_1 of 0.9, β_2 of 0.999, and ϵ of 10^{-8} . For Split CIFAR-100S, we trained ResNet-56 [14] from scratch for 70 epochs using a batch size of 256. For CelebA and Split ImageNet-100, we trained ResNet-18 from scratch for 50 and 70 epochs, respectively, using a batch size of 128. We incorporated the cosine annealing learning rate decay, with the maximum number of iterations set to the same as the number of training epochs.

B.2. Implementations of continual learning methods

In the original Elastic Weight Consolidation (EWC) algorithm [22], the snapshot of a CL model should be stored whenever the model is updated from a new task. This stored model is then used to calculate the importance scores of model parameters in the new task. Namely, the algorithm requires a linearly growing amount of memory to store a sequence of models, which is space-inefficient. To address this issue, we implemented online EWC, proposed in [43], which averages the importance scores in an online manner without storing a set of models.

For Learning Without Forgetting (LWF) [27], we used an average of the distillation losses for each head to balance between the cross entropy loss and the distillation losses.

For Experience Replay (ER) [7], incremental classifier and representation learning (iCaRL) [39] and Packnet [35], we implemented the same as their original versions. For ER, we employed the Reservoir sampling [52] as a strategy for updating the exemplar memory.

Table B.1: **Hyperparameter search ranges.**

Method	Hyperparameter	Search range
EWC [22]	Regularization strength λ	$[10^0, 10^9]$
LWF [27]	Regularization strength λ	$[10^{-2}, 3 \times 10^2]$
ER [7]	Memory size	$[10^{-3}, 10^0]$
iCaRL [39]	Memory size	$[10^{-3}, 10^0]$
PackNet [35]	Pruning ratio r	$[10^{-1}, 8 \times 10^{-1}]$
Group DRO [41]	Learning rate of q	$[10^{-8}, 10^2]$

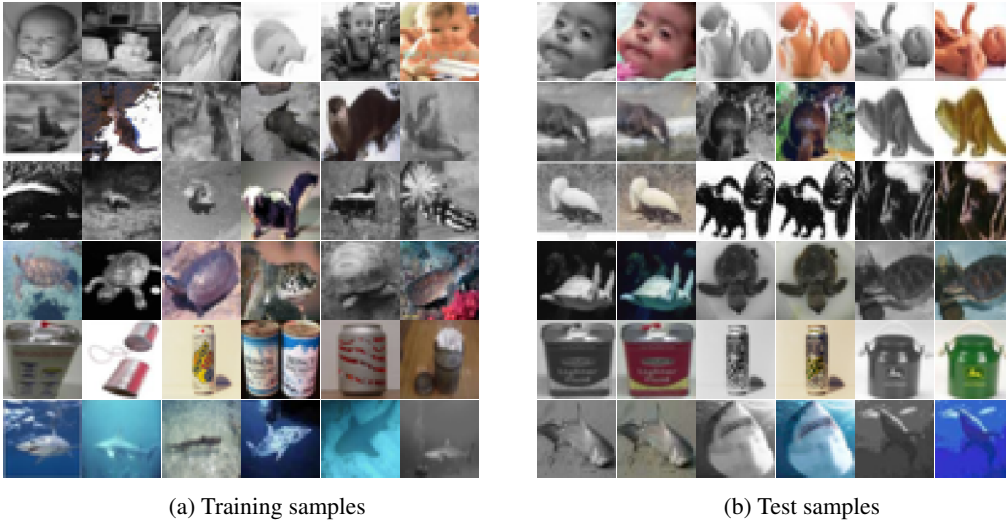


Figure B.1: **Samples in a certain task with bias level of 2 in Split CIFAR-100S.** Each row represents a specific class within the task. The top three rows represent classes biased toward the grayscale samples, while the bottom three rows contain classes biased toward the color samples. The test dataset includes pairs of images, where each pair contains one grayscale and one color version of the same image.

B.3. Hyperparameters for each result

In our experiments, we evaluated CL methods several times by varying their hyperparameters based on the sets of candidates. The candidates are uniformly distributed on a logarithmic scale within a given range. For all figures presented in Section 4 and 5, we then plotted results for some of those hyperparameter candidates. We note that we omitted some overlapped results in Section 4 to enhance visibility. For the table results in Section 6, we tuned the hyperparameters for regularization based methods and Group DRO using the same candidates. We included Table B.1 to provide full ranges of hyperparameters tested. We note that the memory size specified in Table B.1 represents the fraction of the number of training images included in one of all tasks except the last one.

B.4. Datasets

Split CIFAR-100S. In the training dataset of each task, the first five classes are skewed toward the color group and the latter skewed toward the grayscale group, given the skew ratio. For the test dataset of each task, we have pairs of the same images; ones in color, and ones in grayscale. Fig B.1 illustrates some training and test samples in Split CIFAR-100S.

CelebA. Domain-IL typically assumes the input distributions vary as the number of tasks increases. To reflect this assumption in CL scenarios, we divided the CelebA dataset into several tasks based on some selected attributes and each task thereby has different facial features. For instance, the two tasks in CelebA² are defined by whether face images are “smiling” or not. Similarly, we utilize three attributes, “Black Hair”, “Oval Face”, and “Mouth slightly open” for CelebA⁸. By dividing the data in this way, CL scenarios based on CelebA² or CelebA⁸ mimic the distribution shift occurring in real-world applications.

Split ImageNet-100. To study the impact of the watermark bias in CL scenarios, we replace a randomly selected class with

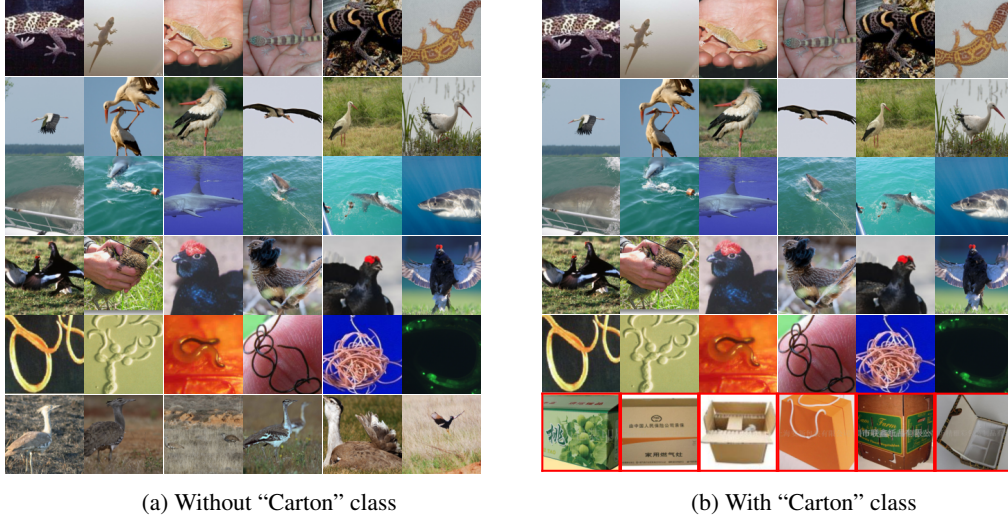


Figure B.2: **Training samples in Split ImageNet-100.** Two plots show training samples in a certain task with different bias levels, *i.e.*, 0 & 6. Each row represents a specific class within the task. The last row of the right plot is the carton class.

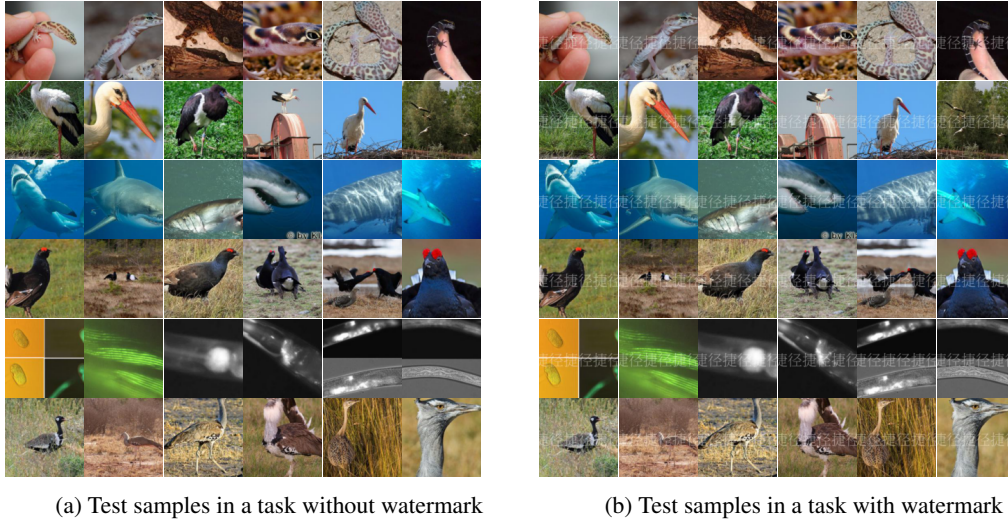


Figure B.3: **Test samples in Split ImageNet-100.** Both sides of samples are used to compute BMR.

the “Carton” class in a certain task. To calculate BMR for the watermark bias, we make watermarked versions of each sample in the original test dataset by the style transfer used in [26]. Examples of training and test samples of Split ImageNet-100 are illustrated in Fig B.2 and B.3.

C. Naive debiasing in CL scenarios

Here, we assume a scenario in which the bias of a model is detected after learning T_1 (stage 1) and T_2 (stage 2) continually. After that, the model is re-trained using existing debiasing techniques to obtain a debiased model (stage 3). For debiasing, we employ an existing debiasing technique, Group DRO, [41] which minimizes the worst-case group loss. For this scenario, we set the bias level of T_1 and T_2 as 0 and 6 respectively. Figure C.1 show the accuracy and BMR of T_2 (left) and T_1 (right) at each stage for each baseline. We plotted the results of each baseline with hyperparameters achieving the highest average accuracy of the two tasks. In the right plot, we observe that some points shift to the bottom left as progressing from stage 1 to stage 2, *i.e.*, forgetting of T_1 . From results of the stage 3 in the left plot, we show that BMR of T_2 can be reduced by Group DRO and MFD. However, we also identify that the accuracy of T_1 significantly drops. Thus, when debiasing after

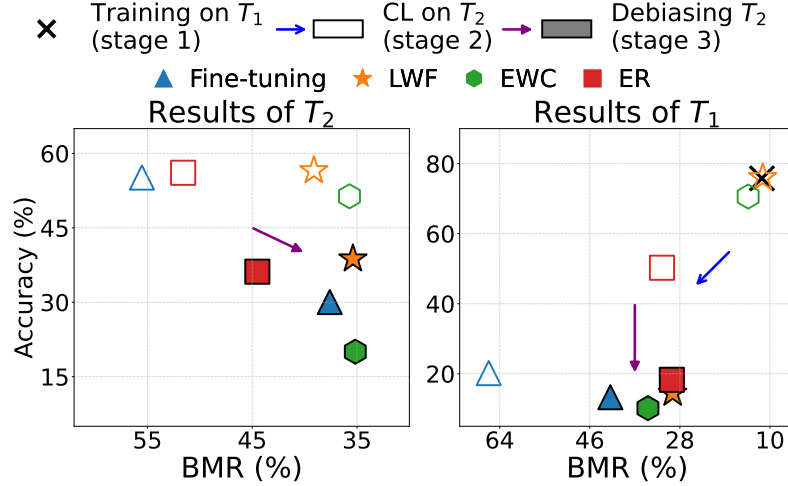


Figure C.1: **Naive debiasing with Group DRO on Split CIFAR-100S.** The accuracy and BMR of T_1 and T_2 are shown for each stage.

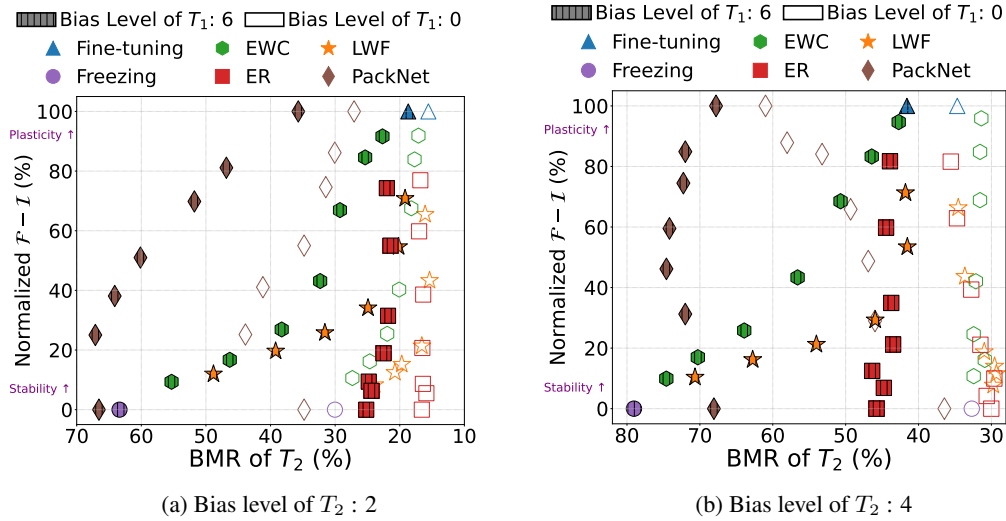


Figure D.1: **Forward transfer of bias in two tasks-continual learning on Split CIFAR-100S.**

learning each task as we argued in Section 4, one should consider forgetting issue of the learned tasks at the same time, *i.e.*, it is necessary to develop a novel debiasing method considering the stability for CL.

D. Additional experimental results

D.1. Forward and backward transfers of bias for CL with two tasks

Figure D.1 displays the forward transfer of the color bias for two task-CLs on Split CIFAR-100S. In each plot in the figure, the bias levels of T_2 are fixed to 2 or 4, respectively, and BMR of T_1 is reported for each CL method and hyperparameter. It is apparent from the figure that the difference in BMR between colored and uncolored points becomes more pronounced with the bias transfer, as compared to results obtained when the bias level of T_2 is fixed to 0. This would be because previously learned biases of a CL model tend to facilitate learning of the dataset bias of the current task more.

Similarly, in Figure D.2, we present the outcomes of two-task experiments for analysis of the backward transfer of bias. As in Figure D.2, the results show that if T_1 already contains a dataset bias, the effect of the backward transfer of the bias from T_2 is more pronounced.

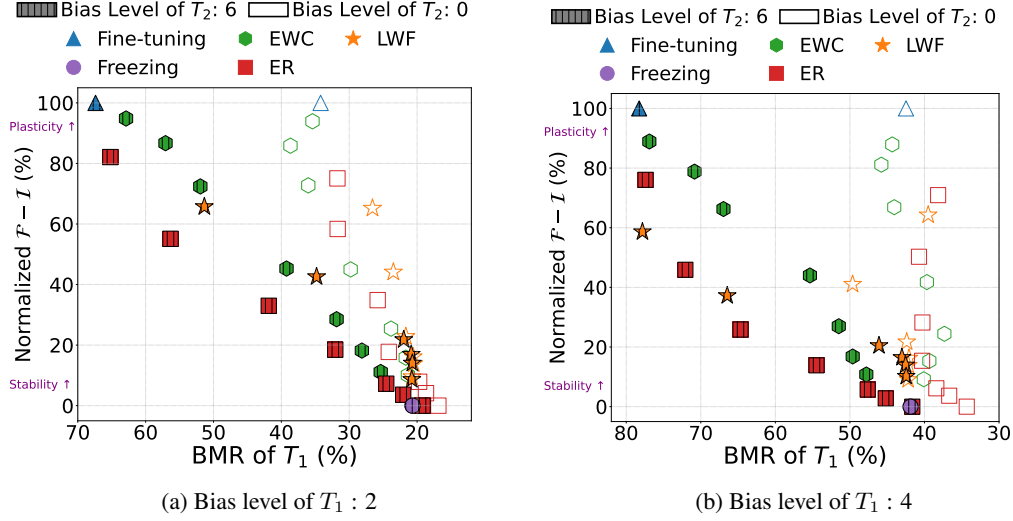


Figure D.2: Backward transfer of bias in two tasks-continual learning on Split CIFAR-100S.

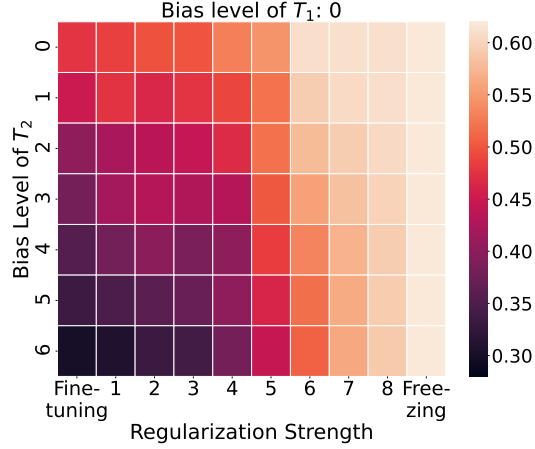


Figure D.3: CKA on Split CIFAR-100S. The CKA values between color images and grayscale images in T_1 are shown. Each value is calculated after learning T_2 by EWC.

D.2. Feature representation analysis for backward transfer of bias

We exhibit the results of CKA analysis for the backward transfer on Split CIFAR-100S. From Figure D.3, we observe a clear trend indicating the CKA value decreases as the regularization strength decreases and the bias level of T_2 increases. This again suggests that when a CL method focuses on learning a biased current task, *i.e.*, plasticity, the backward transfer of bias by a CL method becomes more obvious.

D.3. Experimental results for accuracy with a longer sequence of tasks

Figure D.4 and D.5 show accuracies corresponding to each of the results in Figure 5 and 6 in the manuscript. The figures demonstrate that the accuracies in the same intervals are roughly the same, so we conclude that the gaps of BMR shown in Figure 5 and 6 are due to the bias transfers, not the accuracy gaps.

E. Discussions about results for backward transfer on Split ImageNet-100

In this section, we analyze the predictions of a models in order to investigate why the backward transfer is not observed in Class-IL scenarios with two-tasks on Split ImageNet-100. Table D.1 (resp. Table D.2) represents the CL scenarios for the

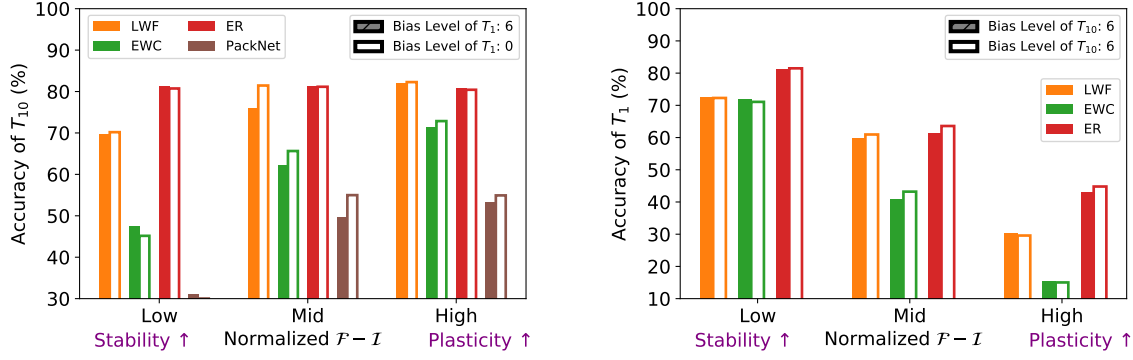


Figure D.4: Accuracy in longer sequences of Split CIFAR-100S. The experimental settings in two plots are the same as in Figure 5(a) and 5(b), respectively.

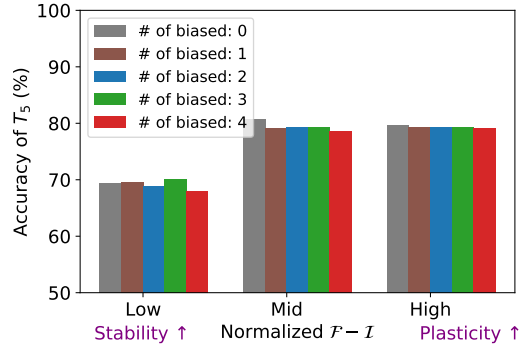


Figure D.5: Accuracy of T_5 depending on the number of biased tasks. The experimental settings are the same as in Figure 6.

Table D.1: Mis-classified ratio of T_2 test data when watermark is added either after learning “carton” in T_1 or not. We reported the results with memory capacity which is 100% of T_1 data to consider the stability.

Prediction	Mis-classified ratio (%)	
	T_1 with “carton”	T_1 without “carton”
Old class	4.52	7.78
New class	7.74	6
“Carton” class (old)	4.02	-
Total (BMR)	16.28	13.78

Table D.2: Mis-classified ratio of T_1 test data when watermark is added either after learning “carton” in T_2 or not. We reported the results with memory capacity which is 10% of T_1 data to consider the plasticity.

Prediction	Mis-classified ratio (%)	
	T_2 with “carton”	T_2 without “carton”
Old class	2.06	1.38
New class	21.61	28.06
“Carton” class (new)	5.69	-
Total (BMR)	29.36	29.44

forward (resp. backward) transfer of bias, which evaluates the bias for T_2 (resp. T_1) by varying the bias level of T_1 (resp. T_2), *i.e.*, whether the “carton” class is contained in the task or not. We employ ER in our experiments and set the memory

size as 1 in Table D.1 or 0.1 in Table D.2, to make forward and backward transfer of bias significantly occurs by focusing more on stability or stability, respectively. To analyze BMR values in more detail, we divided the cases of misclassification of bias-conflicted samples into three categories; a CL model falsely predicts for 1) one of the old classes (except the carton), 2) one of the new classes (except the carton), and 3) the “carton” class.

The following are our observations from the tables. First, we observe that BMRs of T_1 in Table D.2 show almost no difference regardless of whether a CL model learns the “carton” class under high plasticity, while BMR of T_2 increases in Table D.1 when T_1 contains the “carton” class. Namely, in terms of BMR, it looks like the backward transfer of the watermark bias does not occur. However, when we look at the categorized results, we can derive different trends, *i.e.*, the backward transfer still occurs. In Table D.2, when T_2 contains the “carton” class, some samples with the watermark are misclassified into the “carton” class, *i.e.*, the CL model possesses watermark bias in T_1 due to backward transfer. We then argue that the main cause of similar BMRs in Table D.2 would be the *old-new bias*, an inherent issue of Class-IL, which indicates biased predictions towards new classes. Indeed, when the watermark is injected into samples in T_1 which belongs to old classes, we see a disproportionately high ratio of incorrectly predicted samples for the new classes in Table D.2. On the other hand, we observe that the ratios for old and new classes are relatively similar in Table D.1, since the watermark bias is injected to samples in T_2 which belongs to new classes. Thus, we can infer that the old-new bias can make the model predictions for samples in T_1 vulnerable to watermark bias and easily shift to new classes in T_2 , even if the model did not explicitly learn the “carton” class. This explains high misclassified ratios for new class regardless of the dataset bias of T_2 and similar BMRs in Table D.2 although the backward transfer of bias occurs.